Journal of Materials Chemistry A

MXene binder stabilizes pseudocapacitance of conducting polymers

Journal:	*Journal of Materials Chemistry A*
Manuscript ID	TA-COM-07-2021-005861.R1
Article Type:	Communication
Date Submitted by the Author:	11-Aug-2021
Complete List of Authors:	Boota, Muhammad; Drexel University, Department of Materials Science and Engineering Jung, Euiyeon; Drexel University, Department of Materials Science and Engineering Ahuja, Rajeev; Uppsala Universitet, Physics and Astronomy Hussain, Tanveer; The University of Western Australia, School of Molecular Sciences

MXene binder stabilizes pseudocapacitance of conducting polymers

Muhammad Boota[a,‡,*], Euiyeon Jung[a,‡], Rajeev Ahuja[b, c], Tanveer Hussain[d, e]

[a] A. J. Drexel Nanomaterials Institute and Department of Materials Science and Engineering, Drexel University, Philadelphia, PA 19104, USA
[b]Condensed Matter Theory Group, Department of Physics and Astronomy, Box 516, Uppsala University, S-75120 Uppsala, Sweden.
[c]Department of Physics, Indian Institute of Technology Ropar, Rupnagar 140001, Punjab, India
[d] School of Molecular Sciences, The University of Western Australia, Perth, WA, 6009, Australia
[e] School of Chemical Engineering, The University of Queensland, St Lucia, Brisbane, 4072. Australia

[‡]*Equal contribution*
*Corresponding Author E-mail: boota@drexel.edu

Abstract

Conducting polymers (CPs) are by far the most studied organic materials for supercapacitors. Yet, their structural instability stemming from volumetric expansion/contraction during charge/discharge results in capacitance loss after moderate cycling that limits their applications. Here, we show that the remarkable cycling stability, capacitance, and rate performance can be achieved by replacing conventional electrode additives (carbon black or insulating polymer binder) with titanium carbide ($Ti_3C_2T_x$) MXene. Using polyaniline (PANI) as a model system, an addition of only 15 wt% of $Ti_3C_2T_x$ MXene binder delivered remarkable capacitance retention of 96% after 10,000 cycles at 50 mV/s and high-rate capability with a capacitance of 434 F/g. Using density functional theory (DFT) calculations, we show that, unlike insulating polymer binders, surface groups of MXene bond to PANI with a significantly high binding energy (up to -2.11 eV) via a charge transfer mechanism. This is one of the key mechanisms to achieve a high electrochemical performance of the CP-based electrodes when MXene is used as a binder. We expect that a similar approach can be used for stabilizing other organic electrode materials.

Keywords: MXene, conducting polymer, titanium carbide, binder, 2D material, supercapacitor

Introduction

Conducting polymers (CPs) are versatile materials that find applications in a broad range of applications including supercapacitors and batteries.[1,2] They offer intrinsic electronic conductivity (~100–10,000 S/m), facile synthesis, high theoretical capacitance, good flexibility, and potential recyclability.[1,2] CPs such as PANI, polypyrrole, poly(3,4-ethylenedioxythiophene), and their composites have been explored for supercapacitors due to their high pseudocapacitance.[3] However, their high capacitance starts fading upon moderate cycling due to volumetric changes caused by ion doping/undoping during their redox reactions.[4] So far, a large focus to fix this issue was to combine CPs with an array of modestly conductive carbon nanomaterials.[4,5] Conventionally, CP-based electrodes are comprised of CP as an active material, and electrode additives such as carbon black and an insulating polymer binder like polyvinylidene fluoride (PVDF) or polytetrafluoroethylene (PTFE), where the former assists charge transport and later keeps electrode components entangled during electrochemical operation.[1–5] The use of these conventional additives has not yet enabled CPs to achieve their maximum electrochemical performance potentially due to the following reasons[6,7]: (1) polymer binder is an insulating material that hinders the ionic and electronic percolation throughout the electrode, (2) polymer binders are not mechanically strong enough to resist the volume expansion of CP electrodes during electrochemical operation, (3) use of binder negatively impacts the rate performance of the electrodes, and (4) non-uniform distribution of the carbon black particles impedes the smooth transport of the ions/electrons. These issues can be resolved by replacing electrochemically inactive polymer binder and carbon black with a single conductive, flexible, electroactive, and mechanically robust binder.

In search of conductive binders for CP-based supercapacitors, 2D MXene sheets could be a suitable candidate to address the stability of the CP-based supercapacitors. MXenes, a rapidly growing large group of 2D transition metal carbides, nitrides, and carbonitrides, have shown potential for numerous applications, most importantly, for supercapacitors.[8] MXenes—with a general formula of $M_{n+1}X_nT_x$, where M = Ti, V, Mo, Cr, etc.; X = carbon/nitrogen; n = 1, 2, or 3; and T_x = O, OH, and F—are generally synthesized by wet chemical etching of the A element layers from the MAX phases.[9] Although MXenes as binders have shown improved electrochemical performance in carbon-based supercapacitors and metal-ion non-aqueous energy storage systems[6,7,10], they have never been explored to stabilize the pseudocapacitive performance of organic electrodes, particularly CPs, and that is the research area where their use can dramatically solve the long-standing poor conductivity and low cycle life issues of organic materials. MXenes can offer multiple benefits when used as a binder for the stability of the CPs[11]: (1) unlike conventional insulating polymer binder which is a charge barrier within CP-based electrodes, MXene will be a charge carrier due to its metallic conductivity, (2) the flexibility of MXene layers will make processing of the electrodes easier, (3) intrinsic redox capacitance MXene will boost the overall electrochemical performance of the CPs, (4) the high mechanical strength of the MXenes will assist high rate performance, which is usually challenging for the organic electrodes, (5) the functional groups of MXene (-O, -OH, -F, etc.) can potentially bond to the CP surface to induce strong interactions, which may help to enhance the cycle life of the electrodes.

Considering the aforementioned benefits, we introduce $Ti_3C_2T_x$ MXene as a multifunctional binder to replace conventional additives (polymer binder or carbon black) in CP-based electrodes to boost and stabilize the overall electrochemical performance. We selected $Ti_3C_2T_x$ MXene and PANI as our model systems to study their pseudocapacitive performance.

Using DFT calculations, we further provided the bonding, preferential orientation, and charge transfer mechanism between $Ti_3C_2T_x$ MXene and PANI.

Experimental and computational details

$Ti_3C_2T_x$ MXene was synthesized similar to previous reports.[9,12] Briefly, 2g of LiF was solved in a 20 ml HCl solution (9M) followed by gentle addition of the 2g Ti_3AlC_2 MAX powder. While stirring, the solution was heated at 35 °C for 24 h. Subsequently, the mixture was washed with deionized water till pH ~6 to obtain an etched solid. The etched powder was bath sonicated and filtered using a vacuum filtration setup to obtain $Ti_3C_2T_x$ MXene. PANI was synthesized following previous reports.[13,14] A known amount of MXene was introduced to the PANI during in-situ polymerization. The final solution was filtered, washed, and dried. The obtained slurry was directly rolled to obtain ~40 μm MXene-bonded PANI electrodes.

Scanning electron microscope (SEM) images of the samples were collected on Zeiss Supra 50VP (Carl Zeiss AG, Germany). The Fourier-transform infrared (FTIR) spectra were collected on FTIR spectrometer (PerkinElmer) with a resolution of 4 cm^{-1}. Raman spectra were obtained on Renishaw inVia spectrometer (632 nm, 5% laser power). The electrochemical performance of the MXene-bonded PANI film electrodes was tested using cyclic voltammetry (CV) on a VMP3 potentiostat (Biologic, France) in a three-electrode configuration. A ~40 μm freestanding MXene-bonded PANI film served as a working electrode, activated carbon (~100 μm) as a counter electrode, Ag/AgCl as a reference electrode, and glassy carbon as current collectors. All experiments were conducted in 3 M H_2SO_4 electrolyte. The following equation was used to calculate capacitance similar to our previous report[12]:

$$C_s = \int I.dV/\vartheta mV$$

Where C_s is the specific capacitance (F/g), I is the current response, ϑ is the scan rate (mV/s), m is the mass (g), and V is applied potential (V).

For the atomic-scale understanding of the interaction mechanism between MXene ($Ti_3C_2O_2$) and PANI, we used first-principles spin-polarized calculations based on DFT by using VASP code.[15,16] For tackling the electron-ion interactions, generalized gradient approximation (GGA) of Perdew-Burke-Ernzerhof was used and the projector-augmented wave (PAW) method approximated the exchange and correlation.[17,18] A cut-off energy of 600 eV was used throughout the calculations for the plane-waves basis-set. Capturing van der Waals interactions in weakly interacting systems is very important for studying the accurate binding mechanism. Therefore, we incorporated van der Waals correction of Grimme at DFT-D3 level in our calculations.[19] Brillouin zone (BZ) sampling was performed by using KPOINTS mesh under Monkhorst-Pack scheme with a mesh size of 5×5×1.[20] Structural optimization was performed until the total energy and force criteria of 10^{-6} eV and 0.01 eV/ Å were met, respectively. The charge transfer mechanism between $Ti_3C_2O_2$ and PANI was studied using Bader charge analysis.[21]

Results and discussion

Figure 1a is the schematic illustration of producing PANI electrodes in which $Ti_3C_2T_X$ MXene is used as a multifunctional binder. We used the *in-situ* oxidative polymerization method to prepare PANI and introduced a known amount of the pre-synthesized $Ti_3C_2T_x$ MXene suspension during the polymerization process. The idea to introduce MXene during polymerization was to ensure the homogeneous distribution of the conductive MXene sheets that are needed to ensure the charge transport during the electrochemical process. The SEM image of the 85 wt% PANI content (Figure 1b) shows fiber-shaped PANI within electrode having overall an interconnected architecture which is generally favorable for the ion and electron transport.[22]

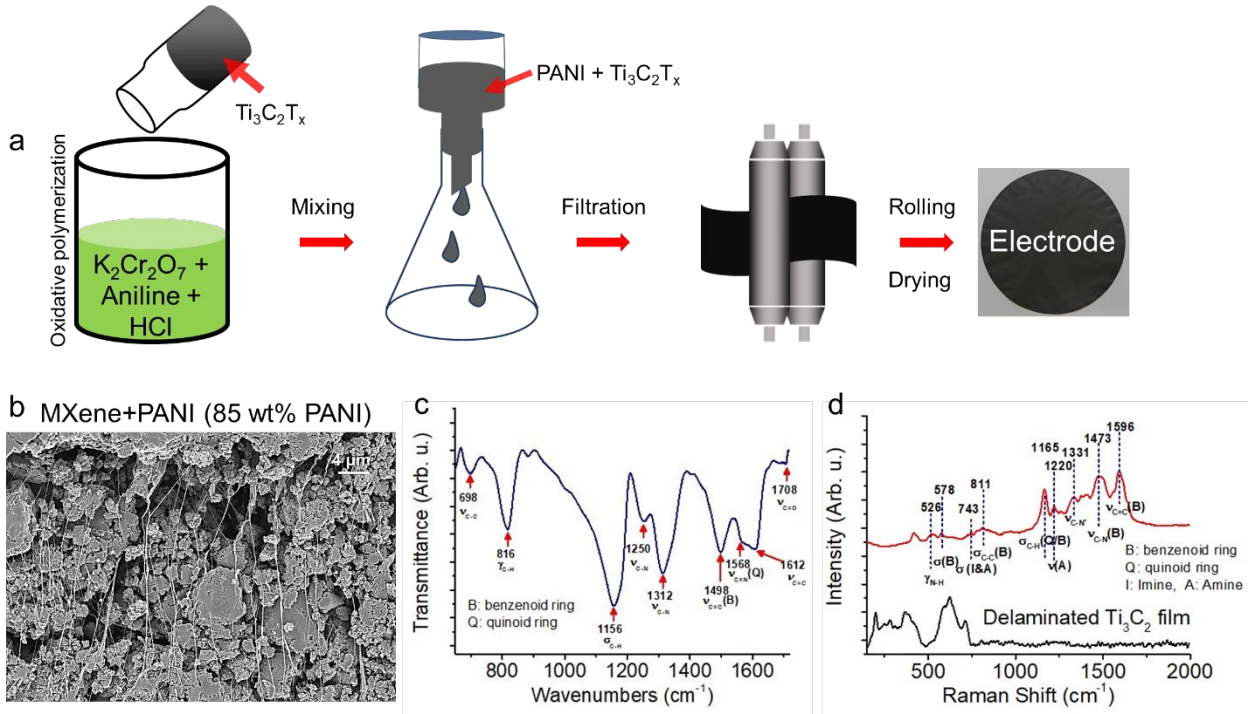

Figure 1. (a) Schematic diagram for the manufacturing of MXene-bonded PANI films; (b) Scanning electron microscope images of MXene bonded PANI film having 15 wt% of $Ti_3C_2T_x$ MXene; (c) Corresponding FTIR; and (d) Raman spectra confirming the formation of PANI.

FTIR bands[23–25] (Figure 1c) at 698, 816, 1156, 1250, 1312, 1498, 1568, 1612, and 1708 cm^{-1} confirmed the PANI polymerization and are ascribed to the C-C stretching, C-H out-of-plane deformation in 1,4-disubstituted benzene, C-H in-plane bending of aromatic, C-N vibrations, C-N stretching of secondary aromatic amine, C=C stretching of benzenoid, C=C stretching of quinonoid, C=C stretching, and C=O stretching, respectively. Raman spectra further corroborated FTIR findings. The Raman bands (Figure 1d) at 526, 578, 743, 811, 1165, 1220, 1331, 1473, 1596, and 1641 are ascribed to N-H out of plane bending, in-plane bending of benzenoid, in-plane bending of imine and amine, C-C in-plane bending of benzenoid, C-H in-plane bending of quinoid/benzenoid with quinoid character, C-N stretching of amine, $C\text{-}N^+$ stretching of bipolaron structure, C-N stretching of benzenoid, C-C stretching of benzenoid, and C=C stretching of benzenoid, respectively.[5,26]

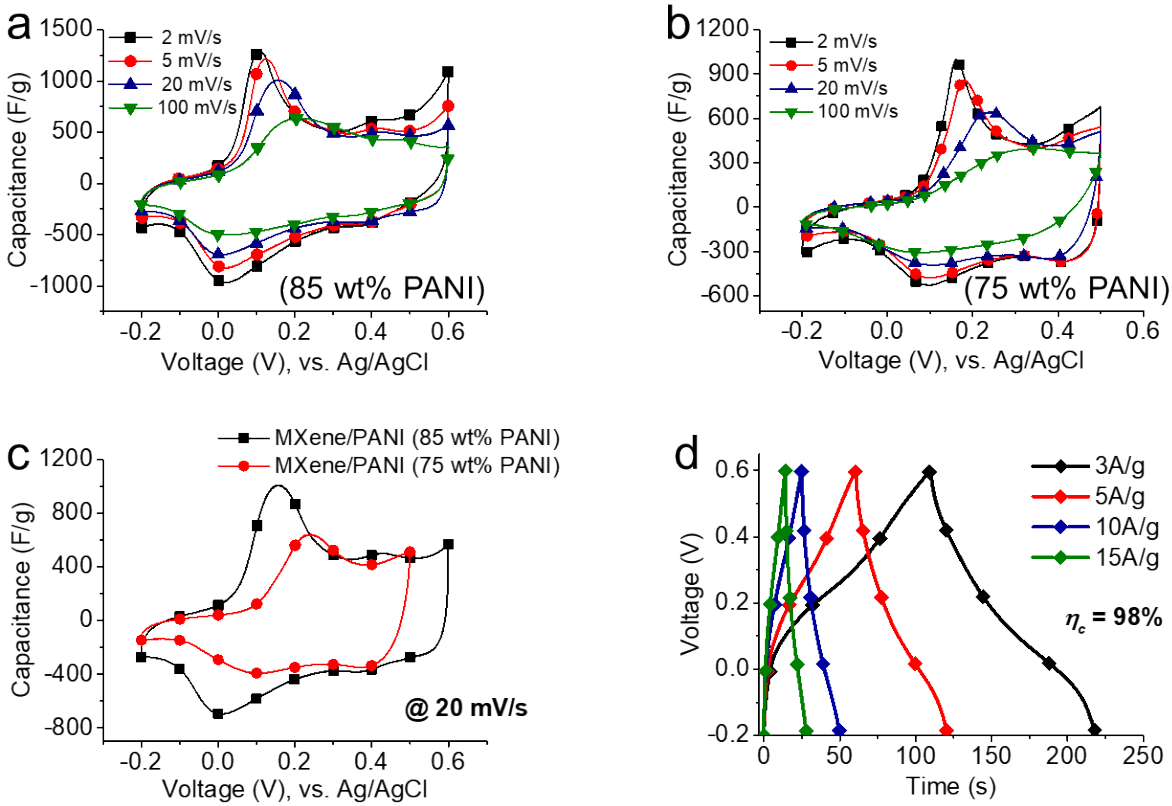

Figure 2. CV curves of 15 wt% MXene-containing PANI electrodes at different scan rates (2-100 mV/s); (b) CV curves of 25 wt% MXene-containing PANI; (c) CV comparison of both compositions (15 and 25 wt%) at 20 mV/s; (d) GCD profiles of 15 wt% MXene bonded PANI at varying current densities.

The charge storage performance of MXene-containing PANI electrodes was tested in a three-electrode configuration in 3 M H_2SO_4. Cyclic voltammograms (CVs) of the 15 wt% MXene binder electrodes (Figure 2a) at different scan rates (2–100 mV/s) in the potential range of -0.2 to 0.6 V showed two distinct redox peaks, consistent with the redox transition of PANI between leucoemeraldine/emeraldine and emeraldine/pernigraniline.[5,27]

When the MXene-binder was increased to 25 wt%, the oxidation of the MXene became an issue and the cut-off potential was reduced to 0.5 V to maintain stable performance (Figure 2b). This shows that the optimal amount for the MXene binder is 15 wt% which is matched or even lesser to the case of conventional CP-based electrodes comprising PVDF/PTFE or activated

carbons as electrode additives.[28] Figure 2c further shows the voltage stability comparison for the 15 (0.6 V) and 25 wt% (0.5 V) MXene binder within the electrode. Galvanostatic charge/discharge (GCD) plots of 15 wt% MXene composition (Figure 2d) at different current densities (3-15 A/g) showed symmetric charge/discharge, confirming good redox reversibility and high Coulombic efficiency (~98%).

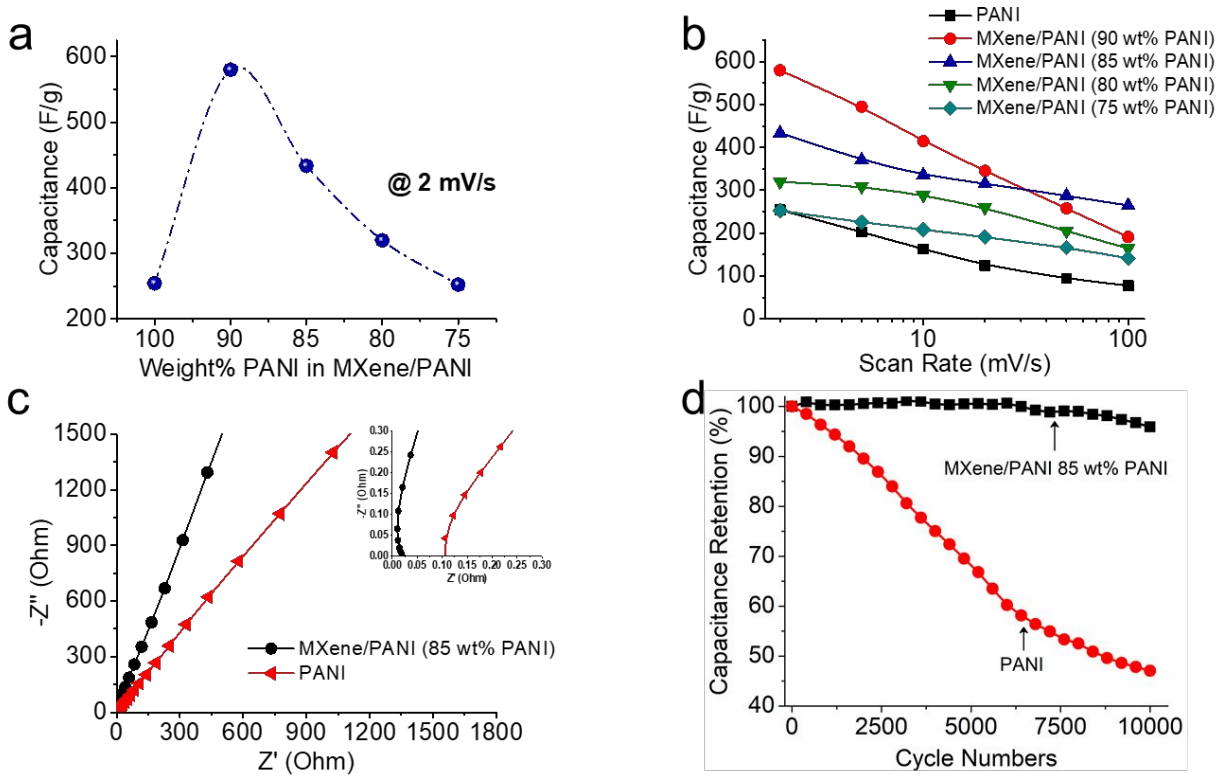

Figure 3. (a) Effect of MXene binder on gravimetric capacitance calculated at 2 mV/s; (b) Effect of varying MXene loadings on rate performance of MXene bonded PANI electrodes; (c) Nyquist plot of optimized composition with pristine PANI electrodes; (d) Cycling stability of 15 wt% MXene with pristine PANI electrodes.

We tested multiple binder compositions to identify the optimum amount of the MXene binder, and the effect of the MXene binder on capacitance is plotted in Figure 3a. A capacitance of 580 F/g was achieved when the MXene binder content was 10 wt%, which gradually declined to 434, 320, and 252 F/g when the MXene content was increased to 15, 20, and 25 wt%, respectively. The highest capacitance is 2.3 times higher than conventional PANI electrodes

(PANI + PTFE + activated carbon) due to the synergetic contributions of the PANI and MXene.[29] When the rate performance was plotted (Figure 4b), it became clear that the 15 wt% MXene content delivered the best rate performance. Although 10 wt% MXene composition showed the highest capacitance of 580 F/g at 2 mV/s, it sharply declined at higher scan rates. At a scan rate of 100 mV/s, the 10 wt% binder compositions showed a ~27% higher decline in capacitance compared to their 15 wt% counterparts. The Nyquist plot derived from the electrochemical impedance spectroscopy (Figure 4c) showed a vertical line in the low-frequency region which is an attribute of capacitive behavior.[30] The use of conductive MXene as a binder reduced the ohmic resistance and diffusion resistance compared to its conventional pristine counterpart as seen in the high-frequency region of the Nyquist plot (Figure 4c, inset).

We performed a cycle life test on the 15 wt% MXene binder composition film up to 10,000 cycles at a scan rate of 50 mV/s (Figure 3d). The addition of the 15 wt% binder delivered excellent capacitance retention of 96% after 10,000 cycles, outperforming many PANI-containing composite electrodes in which conventional binders were used.[31–34] The conventional PANI electrodes lost more than half of their initial capacitance showing only 47% capacitance retention. This clearly shows that the MXene binder not only boosted the capacitance but also stabilized the cycling performance of the PANI electrodes. To the best of our knowledge, this capacitance retention value is one of the best obtained for any new tested organic or inorganic binder for CP or organic electrodes.

For the atomic-scale understanding of the interaction mechanism between MXene ($Ti_3C_2O_2$) and PANI, we further used first-principles spin-polarized calculations based on DFT. We considered two units of the PANI which consisted of 26 atoms in total (C=H=12, N=2). We found a 4×4×1 supercell of $Ti_3C_2O_2$ (Ti=48, C=O=32), sufficient enough to bind PANI. Several

bindings sites exist on $Ti_3C_2O_2$ for the adsorption of PANI. Similarly, PANI can bind/adsorb in several different alignments (e.g., parallel, vertical, and tilted orientations towards the $Ti_3C_2O_2$).

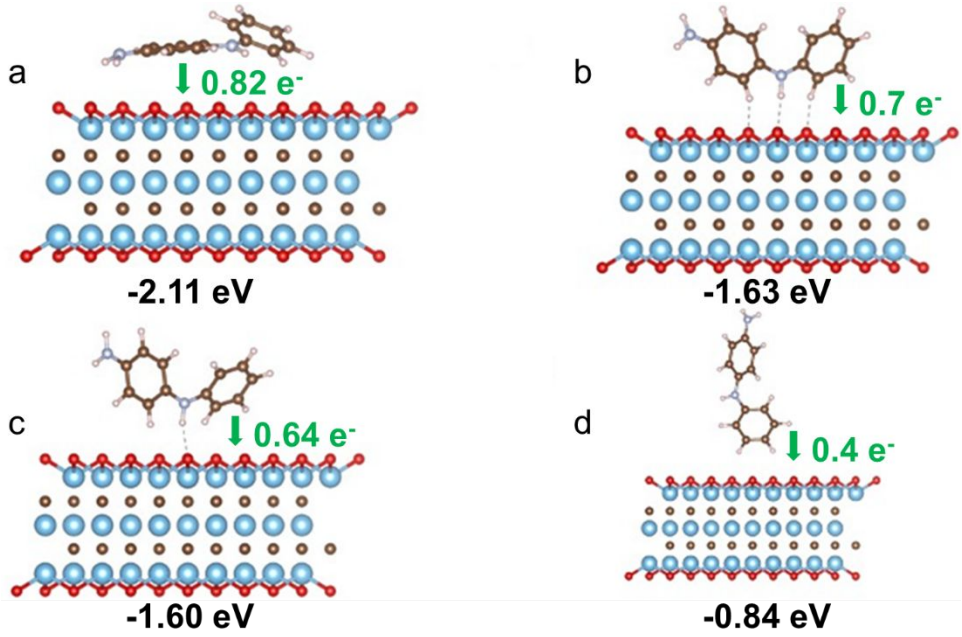

Figure 4. Optimized structures of different PANI adsorbed $Ti_3C_2O_2$ configurations. Blue, brown, red, and pink balls represent Ti, C, O, and H atoms, respectively.

To attain the most stable PANI-adsorbed $Ti_3C_2O_2$ structure (PANI@$Ti_3C_2O_2$), we considered several initial configurations and allowed the systems to optimize completely without any constraints. Complete geometry optimization yielded the four PANI@$Ti_3C_2O_2$ configurations as shown in Figure 4. Binding energies (E_b) of PANI with $Ti_3C_2O_2$ were calculated by the following equation:

$$E_b = E\,(Ti_3C_2O_2@PANI) + X - E\,(Ti_3C_2O_2) - E\,(PANI)$$

The first, second, and third terms on the right-hand side of the above equation represent the total energies of PANI doped $Ti_3C_2O_2$, pristine $Ti_3C_2O_2$, and PANI molecule, respectively. The binding energies were found to be -2.11, -1.63, -1.60, and -0.84 eV for configurations shown in Figure 4a, b, c, and d, respectively. The E_b values indicated that the PANI preferred to sit over the $Ti_3C_2O_2$ surface horizontally (Figure 4a). The optimized minimum binding distances (Δd) between PANI

and $Ti_3C_2O_2$ were found as 2.04, 1.97, 1.99, and 2.96 Å, respectively. To further understand the origin of the binding mechanism between PANI and $Ti_3C_2O_2$, we performed Bader charge analysis. We found that the direction of charge transfer was from PANI to $Ti_3C_2O_2$. A thorough investigation revealed that 0.82, 0.7, 0.64, and 0.4 electrons were transferred to $Ti_3C_2O_2$ by a, b, c, and d configurations shown in figure 4. From Bader analysis, it was clear that the higher the charge transfer is from PANI to $Ti_3C_2O_2$, the stronger the binding is.

Based on the experimental and theoretical findings, the overall improved electrochemical performance can be ascribed to: (1) The use of MXene enabled the construction of the 3D interconnected electrode architecture of homogeneously dispersed MXene within PANI molecules that gave continuous conductive pathways for the rapid redox reactions, (2) charge transfer-induced strong interactions between MXene and PANI molecules kept electrode intact during electrochemical cycling that yielded high capacitance retention, (3) opposed to conventional additives which provide point contact with the electrode material, the high aspect ratio and 2D nature of the MXene provided continue paths for the PANI bindings which remained beneficial for the ion and electron transport throughout the electrodes. Moreover, the mechanical strength of the MXene sheets significantly improved the mechanical robustness of the PANI electrodes which significantly enhanced the overall electrochemical performance. (4) pristine $Ti_3C_2T_x$ MXene has already proven as an outstanding pseudocapacitive material with exceptional cycling performance[9], the use of such material as a conductive additive helped to improve the capacitance and cycle life of the PANI electrodes.

Conclusions

In conclusion, we have shown that by replacing the conventional additives (polymer binders such as PVDF or PTFE and carbon black) in CP-based electrodes with $Ti_3C_2T_x$ MXene, we can achieve

both high capacitance and excellent cycling stability. Among many tested compositions of the MXene binder, a binder-free ~40 μm thick electrodes having 15 wt% MXene delivered a high capacitance of 434 F/g at 2 mV/s, good rate performance, and excellent capacitance retention of 96% after 10,000 cycles. In contrast, pristine PANI electrodes lost over 50% capacitance under similar cycling conditions. The improved electrochemical performance stems from the metallic conductivity and mechanical robustness of intrinsically pseudocapacitive MXene along with its tendency to strongly bind organic molecules. Based on DFT calculations, we showed that the excellent performance of the MXene-containing PANI electrodes comes from the fact that PANI molecules strongly bond to the MXene surface with binding energies as high as -2.11 eV. In addition, there is a significant amount of charge transfer from PANI to MXene (up to 0.82 electrons). High binding energy and charge transfer kept PANI and MXene entangled over the long cycling without any significant capacitance fade. With a wide array of MXenes available, we believe that MXene can solve the poor stability and conductivity issues faced by the organic electrodes, enabling commercial organic energy storage devices (batteries, supercapacitors) with a low environmental footprint.

Conflicts of interest

There are no conflicts to declare.

Acknowledgments

The authors thank Prof. Yury Gogotsi for guiding this work. This work was supported as part of the Fluid Interface Reactions, Structures and Transport (FIRST) Center, an Energy Frontier Research Center funded by the U.S. Department of Energy, Office of Science, and Office of Basic Energy Sciences. R.A. thanks the Swedish Research Council (VR-2016-06014 & VR-2020-04410) and J. Gust. Richert stiftelse, Sweden (2021-00665) for financial support. SNIC, HPC2N, at Sweden is acknowledged for providing the computing facilities.

Notes and references

1 T. Liu, L. Finn, M. Yu, H. Wang, T. Zhai, X. Lu, Y. Tong and Y. Li, *Nano Lett.*, 2014, **14**, 2522–2527.
2 M. Boota, B. Anasori, C. Voigt, M.-Q. Zhao, M. W. Barsoum and Y. Gogotsi, *Adv. Mater.*, 2015, **28**, 1517–22.
3 G. A. Snook, P. Kao and A. S. Best, *J. Power Sources*, 2011, **196**, 1–12.
4 Q. Meng, K. Cai, Y. Chen and L. Chen, *Nano Energy*, 2017, **36**, 268–285.
5 M. Boota, M. P. Paranthaman, A. K. Naskar, Y. Li, K. Akato and Y. Gogotsi, *ChemSusChem*, 2015, **8**, 3576–3581.
6 L. Yu, L. Hu, B. Anasori, Y.-T. Liu, Q. Zhu, P. Zhang, Y. Gogotsi and B. Xu, *ACS Energy Lett.*, 2018, **3**, 1597–1603.
7 C. J. Zhang, S.-H. Park, A. Seral-Ascaso, S. Barwich, N. McEvoy, C. S. Boland, J. N. Coleman, Y. Gogotsi and V. Nicolosi, *Nat. Commun.*, 2019, **10**, 1–9.
8 Y. Gogotsi and B. Anasori, *ACS Nano*, 2019, **13**, 8491–8494.
9 M. Ghidiu, M. R. Lukatskaya, M.-Q. Zhao, Y. Gogotsi and M. W. Barsoum, *Nature*, 2014, **516**, 78–81.
10 N. Sun, Q. Zhu, B. Anasori, P. Zhang, H. Liu, Y. Gogotsi and B. Xu, *Adv. Funct. Mater.*, 2019, **29**, 1906282.
11 M. Boota, C. Chen, K. L. Van Aken, J. Jiang and Y. Gogotsi, *Nano Energy*, 2019, **65**, 104022.
12 M. Boota, C. Chen, L. Yang, A. I. Kolesnikov, N. C. Osti, W. Porzio, L. Barba and J. Jiang, *Chem. Mater.*, 2020, **32**, 7884–7894.
13 M. P. Kumar, L. M. Lathika, A. P. Mohanachandran and R. B. Rakhi, *ChemistrySelect*, 2018, **3**, 3234–3240.
14 P. Chowdhury and B. Saha, *Indian J. Chem. Technol.*, 2005, **12**, 671–675.
15 G. Kresse and J. Hafner, *Phys. Rev. B*, 1993, **47**, 558–561.
16 G. Kresse and J. Hafner, *Phys. Rev. B*, 1994, **49**, 14251–14269.
17 J. P. Perdew, K. Burke and M. Ernzerhof, *Phys. Rev. Lett.*, 1996, **77**, 3865–3868.
18 P. E. Blöchl, *Phys. Rev. B*, 1994, **50**, 17953–17979.
19 S. Grimme, J. Antony, S. Ehrlich and H. Krieg, *J. Chem. Phys.*, 2010, **132**, 154104.
20 H. J. Monkhorst and J. D. Pack, *Phys. Rev. B*, 1976, **13**, 5188–5192.
21 R. F. W. Bader, *Atoms in Molecules: A Quantum TheoryNo Title*, Oxford University Press, Oxford, UK, 1990.
22 H. Sun, L. Mei, J. Liang, Z. Zhao, C. Lee, H. Fei, M. Ding, J. Lau, M. Li, C. Wang, X. Xu, G. Hao, B. Papandrea, I. Shakir, B. Dunn, Y. Huang and X. Duan, *Science*, 2017, **356**, 599–604.
23 N. V Blinova, J. Stejskal, M. Trchová, J. Prokeš and M. Omastová, *Eur. Polym. J.*, 2007, **43**, 2331–2341.
24 C. Li, J. Wang, Y. Wen, Y. Ning, Y. Wen, X. Yuan, M. Li and D. Yang, *ECS Electrochem. Lett.*, 2012, **2**, H1.
25 A. Abdolahi, E. Hamzah, Z. Ibrahim and S. Hashim, *Materials (Basel).*, 2012, **5**, 1487–1494.
26 D. N. Huyen, N. T. Tung, N. D. Thien, L. H. Thanh and others, *Sensors*, 2011, **11**, 1924–1931.
27 Y. Y. Smolin, K. L. Van Aken, M. Boota, M. Soroush, Y. Gogotsi and K. K. S. Lau, *Adv. Mater. Interfaces*, 2017, **4**, 1601201.
28 Q. Abbas, D. Pajak, E. Frąckowiak and F. Béguin, *Electrochim. Acta*, 2014, **140**, 132–138.
29 M. Boota, P. Urbankowski, W. Porzio, L. Barba, N. C. Osti, M. Bleuel, J. K. Keum and E. Mamontov, *ACS Appl. Energy Mater.*, 2020, **3**, 4127–4133.
30 F. Fusalba, P. Gouérec, D. Villers and D. Bélanger, *J. Electrochem. Soc.* , 2001, **148**, A1–A6.
31 F. Hu, W. Li, J. Zhang and W. Meng, *J. Mater. Sci. Technol.*, 2014, **30**, 321–327.
32 Z. Tong, Y. Yang, J. Wang, J. Zhao, B. L. Su and Y. Li, *J. Mater. Chem. A*, 2014, **2**, 4642–4651.
33 H. P. Cong, X. C. Ren, P. Wang and S. H. Yu, *Energy Environ. Sci.*, 2013, **6**, 1185–1191.
34 J. Xu, K. Wang, S. Z. Zu, B. H. Han and Z. Wei, *ACS Nano*, 2010, **4**, 5019–5026.